https://dx.doi.org/10.21577/0103-5053.20210094

J. Braz. Chem. Soc., Vol. 32, No. 11, 2033-2046, 2021

Article

Molecular Structure Studies on Allyl Sulfonamides: Synthesis, Theoretical Treatment and Evaluation of Biological Activity

Anderson S. Rabello,[a] Mayura M. M. Rubinger,[,a] Rafael A. C. Souza,[b] Silvana Guilardi,[b] Guilherme F. de Lima,[c] Eder C. Tavares,[d] Édipo P. Zanon,[#,a] Giovanna R. N. Silva,[a] Laércio Zambolim[e] and Javier Ellena[f]*

[a]*Departamento de Química, Universidade Federal de Viçosa, 36570-977 Viçosa-MG, Brazil*

[b]*Instituto de Química, Universidade Federal de Uberlândia, 38408-100 Uberlândia-MG, Brazil*

[c]*Instituto de Ciências Exatas, Universidade Federal de Minas Gerais, 31270-910 Belo Horizonte-MG, Brazil*

[d]*Instituto de Física e Química, Universidade Federal de Itajubá, 37500-906 Itajubá-MG, Brazil*

[e]*Departamento de Fitopatologia, Universidade Federal de Viçosa, 36570-977 Viçosa-MG, Brazil*

[f]*Instituto de Física de São Carlos, Universidade de São Paulo, 13566-590 São Carlos-SP, Brazil*

Two series of allyl sulfonamides, prepared from Morita-Baylis-Hillman adducts and primary aromatic sulfonamides, were fully characterized. The *Z* configuration for the products derived from 2-[hydroxy(phenyl)methyl]acrylonitrile (**1**) and *E* configuration for those derived from methyl 2-[hydroxy(phenyl)methyl]acrylate (**2**) were confirmed by X-ray diffraction for one compound of each series (**1e**, **2f**). Density functional theory calculations for all allyl sulfonamides agreed with the X-ray crystallographic data. X-ray diffraction studies indicate that these compounds form dimers in their crystal structures. Fingerprint plots show that compound **1e** is stabilized by H···H, C···H/H···C, O···H/H···O and N···H/H···N interactions, while the compound **2f** has no N···H/H···N contacts. Hirshfeld surface analyses were performed to gain insight into the behavior of these interactions. Calculated frontier orbitals showed that their highest occupied and lowest unoccupied molecular orbitals are antibonding orbitals. The allyl sulfonamides **1e** and **2f** are among the most active compounds in each series, inhibiting approximately 60% of the mycelial growth of *Botrytis cinerea* at 3 mmol L^{-1}.

Keywords: sulfonamides, X-ray crystallography, Hirshfeld surface, frontier molecular orbitals, *Botrytis cinerea*

Introduction

Sulfonamides are known mainly for their action against bacteria.[1] Nevertheless, structural modifications and additions of other synthetic blocks to sulfonamides can lead to compounds with different biological properties such as antiglaucoma, antifungal and aldose reductase inhibition.[2-4] The Morita-Baylis-Hillman (MBH) reaction is an important strategy for the formation of carbon-carbon bonds in organic synthesis.[5] The reaction provides polyfunctionalized molecules which can be used as chemical intermediates in the construction of biologically active substances.[3,6-9]

*e-mail: mayura@ufv.br

[#]Present address: Departamento de Ciências Agrárias, Universidade Federal de São João del-Rey, 35701-970 Sete Lagoas-MG, Brazil.

This work presents synthetic and theorical approaches on allyl sulfonamides derived from MBH adducts (Scheme 1). The new allyl sulfonamides, bearing different aromatic substituents linked to the sulfonyl group, were characterized by high-resolution electrospray ionization mass spectrometry (HRMS-ESI), infrared (IR) and nuclear magnetic resonance (NMR) spectroscopies, and by density functional theory (DFT) calculations. In addition, the structures of compounds **1e** and **2f** (Scheme 1) were determined by X-ray diffraction, and Hirshfeld surface analyses were performed for intermolecular interaction studies.

The effects of the allyl sulfonamides **1a-1f** and **2a-2f** (Scheme 1) on the mycelial growth of *Botrytis cinerea* were evaluated *in vitro*. The screening for new antifungals is important to increase the structural variety of chemicals available for field applications to control fungal diseases,

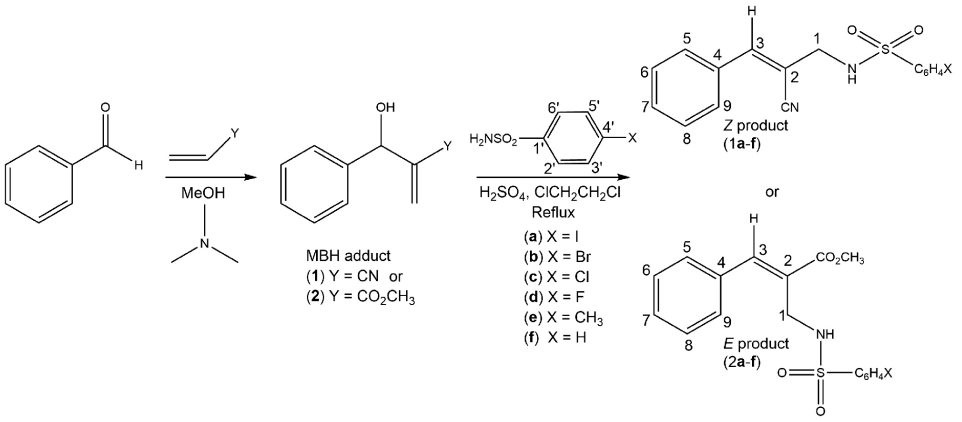

Scheme 1. Syntheses of **1a-1f** and **2a-2f** and numbering for NMR signals attributions.

specially due to the constant emergence of resistant phenotypes.[10] *B. cinerea*, also known as gray mold, affects hundreds of plants species, being the main cause of losses in strawberry and grape crops.[11,12] It can also affect humans, occasionally causing occupational pneumonitis in wine makers and farmers.[13]

Experimental

Methods and materials

Uncorrected melting points (mp) were determined with a MQAPF-302 equipment (Microquímica, Palhoça, Brazil). High resolution mass spectra (HRMS) were recorded in acetonitrile solutions by the direct infusion method, under electrospray ionization (ESI) in the negative mode, on a MicroTOF-QII-ESI-Qq-TOF liquid chromatography mass spectrometer (Bruker Daltonics, Billerica, USA). The IR spectra (4000-500 cm^{-1}) were recorded on a Fourier-transform IR spectroscopy equipment (Varian 660, Palo Alto, USA) by attenuated total reflection (ATR). The ^{1}H (300 MHz) and ^{13}C (75 MHz) NMR spectra were recorded on a spectrophotometer (Varian 300, Palo Alto, USA) using $CDCl_3$ with tetramethylsilane (Sigma-Aldrich, St. Louis, USA) as internal standard. Benzenesulfonamide, 4-chlorobenzenesulfonamide, 4-fluorobenzenesulfonyl chloride, 4-bromobenzenesulfonyl chloride and 4-iodobenzenesulfonyl chloride were purchased from Sigma-Aldrich (St. Louis, USA). The R-sulfonamides (R = 4-fluorophenyl, 4-bromophenyl and 4-iodophenyl) were prepared under reflux by the reaction of the corresponding R-sulfonyl chlorides (Sigma-Aldrich, St. Louis, USA) with concentrated ammonia aqueous solution (Vetec Química Fina Ltda, Duque de Caxias, Brazil). The Morita-Baylis-Hillman adducts were prepared from benzaldehyde with acrylonitrile (for **1**) or methyl acrylate (for **2**), catalyzed by trimethylamine in methanol (Vetec Química Fina Ltda, Duque de Caxias, Brazil) as described in the literature,[3,14] generating the adducts 2-[hydroxy(phenyl)methyl]acrylonitrile (**1**) and methyl 2-[hydroxy(phenyl)methyl]acrylate (**2**). Concentrated sulfuric acid, sodium sulfate and the solvents hexane, 1,2-dichloroethane, ethyl acetate, dichloromethane, chloroform, petroleum ether and acetone were purchased from LabSynth (Diadema, Brazil) and were used without purification. Silica gel for column chromatography and silica gel 60 F254 thin-layer chromatography (TLC) plates were purchased from Sigma-Aldrich (St. Louis, USA).

Syntheses

The syntheses of the (*Z*)-*N*-(2-cyano-3-phenylallyl)-4-X-benzenesulfonamide (**1a-1f**) and methyl (*E*)-3-phenyl-2-(4-X-phenylsulfonamidomethyl)acrylate (**2a-2f**) (Scheme 1), were performed according to the general procedure: concentrated sulfuric acid (54 μL) was dissolved in 1 mL of 1,2-dichloroethane and this solution was added dropwise to a solution of the MBH adduct **1** or **2** (1.0 mmol) and the appropriate benzenesulfonamide (**a-f**, 1.5 mmol) in 1,2-dichloroethane (5 mL), at room temperature (ca. 25 ºC). After stirring under reflux for 2-6 h (monitored by TLC), the reactions were completed. Then, water (10 mL) was added and the product was extracted with 1,2-dichloroethane (3 × 10 mL). The organic phase was dried over sodium sulfate, filtered, and concentrated under reduced pressure. The crude material was purified by column chromatography on silica gel (hexane:ethyl acetate:dichloromethane, 3:1:3), yielding the products **1a**-**1f** (43-72%) and **2a**-**2f** (56-89%). The melting points and spectroscopic data for compounds **1b**-**1f** and **2e** were in accordance with the literature.[3,14] Recrystallization from chloroform/petroleum ether and acetone/water furnished white crystals for **1e** and **2f** (uncorrected mp 143.9-144.5 and 102.2-102.5 °C, respectively) suitable for the X-ray crystallographic analysis. The data for the unpublished allyl sulfonamides are as follows.

(*Z*)-*N*-(2-Cyano-3-phenylallyl)-4-iodobenzenesulfonamide (**1a**)

Yield 43%; white solid; mp 145.2-145.6 °C; IR (ATR) ν_{max} / cm^{-1} 3253, 3057, 2958, 2924, 2854, 2216, 1450, 1414, 1315, 1288, 1138, 1074, 872, 829, 690, 584, 526, 415; ^{1}H NMR (300 MHz, $CDCl_3$) δ 3.81 (d, 2H, *J* 3.0 Hz, H1), 7.29 (s, 1H, H3), 7.44-7.48 (m, 3H, H6, H7 and H8), 7.57 (d, 2H, *J* 9.0 Hz, H2' and H6'), 7.59-7.63 (m, 2H, H5 and H9), 7.95 (d, 2H, *J* 9.0 Hz, H3' and H5'), 8.45 (t, 1H, *J* 3.0 Hz, NH); ^{13}C NMR (75 MHz, $CDCl_3$) δ 47.0 (C1), 101.5 (C4'), 108.4 (C2), 118.3 (CN), 129.0 (C2' and C6'), 129.2 (C5 and C9), 129.6 (C6 and C8), 131.3 (C7), 133.5 (C4), 138.9 (C3' and C5'), 140.9 (C1'), 146.0 (C3); HRMS (ESI) *m/z*, calcd. for $C_{16}H_{12}N_2O_2SI^-$: 422.9664, found: 422.6913.

Methyl (*E*)-2-{[(4-iodophenyl)sulfonamido]methyl}-3-phenylacrylate (**2a**)

Yield 72%; white solid; mp 103.5-104.4 °C; IR (ATR) ν_{max} / cm^{-1} 3261, 3080, 3048, 2945, 1724, 1320, 1223, 1203, 1164, 734, 609; ^{1}H NMR (300 MHz, $CDCl_3$) δ 3.76 (s, 3H, OCH$_3$), 3.99 (d, *J* 6.6 Hz, 2H, H1), 5.31 (t, *J* 6.3 Hz, 1H, NH), 7.30-7.44 (m, 5H, H5, H6, H7, H8 and H9), 7.46 (d, *J* 8.4 Hz, 2H, H2' and H6'), 7.74 (s, 1H, H3), 7.80 (d, *J* 8.7 Hz, 2H, H3' and H5'); ^{13}C NMR ($CDCl_3$, 75 MHz) δ 40.4 (C1), 52.4 (OCH$_3$), 100.0 (C4'), 126.2 (C2), 128.6 (C5 and C9), 128.8 (C6 and C8), 129.4 (C2' and C6'), 129.6 (C7), 133.7 (C4), 138.2 (C3' and C5'), 139.2 (C1'), 143.6 (C3), 167.6 (C=O); HRMS (ESI) *m/z*, calcd. for $C_{17}H_{15}O_4NSI^-$: 455.9767, found: 455.9714.

Methyl (*E*)-2-{[(4-bromophenyl)sulfonamido]methyl}-3-phenylacrylate (**2b**)

Yield 80%; white solid; mp 89.6-90.6 °C; IR (ATR) ν_{max} / cm^{-1} 3255, 3101, 2991, 2945, 1728, 1638, 1327, 1172, 745, 612, 547; ^{1}H NMR (300 MHz, $CDCl_3$) δ 3.74 (s, 3H, OCH$_3$), 3.99 (d, *J* 6.6 Hz, 2H, H1), 5.30 (t, *J* 6.3 Hz, 1H, NH), 7.36-7.41 (m, 4H, H5, H9, H6 and H8), 7.42-7.44 (m, 2H, H3' and H5'), 7.53-7.61 (m, 1H, H7), 7.73 (s, 1H, H3), 7.76-7.82 (m, 2H, H2' and H6'); ^{13}C NMR (75 MHz, $CDCl_3$) δ 40.5 (C1), 52.3 (OCH$_3$), 126.4 (C2), 127.2 (C6 and C8), 128.8 (C5 and C9), 129.0 (C2' and C6'), 129.5 (C3' and C5'), 129.54 (C7), 132.7 (C4), 133.8 (C4'), 139.5 (C1'), 143.5 (C3), 167.6 (C=O); HRMS (ESI) *m/z*, calcd. for $C_{17}H_{15}O_4NSBr^-$: 409.9885 and 407.9905, found: 409.9851 and 407.9893.

Methyl (*E*)-2-{[(4-chlorophenyl)sulfonamido]methyl}-3-phenylacrylate (**2c**)

Yield 81%; white solid; mp 64.5-66.0 °C; IR (ATR) ν_{max} / cm^{-1} 3272, 3080, 3058, 3025, 2948, 2846, 1704, 1332, 1160, 1090, 824, 755; ^{1}H NMR (300 MHz, $CDCl_3$) δ 3.76 (s, 3H, OCH$_3$), 3.99 (d, *J* 6.0 Hz, 2H, H1), 5.34 (t, *J* 6.0 Hz, 1H, NH), 7.33-7.41 (m, 7H, H5, H6, H7, H8, H9, H3' and H5'), 7.68 (s, 1H, H3), 7.71-7.74 (m, 2H, H2' and H6'); ^{13}C NMR (75 MHz, $CDCl_3$) δ 40.4 (C1), 52.3 (OCH$_3$), 126.3 (C2), 128.7 (C6 and C8), 128.8 (C5 and C9), 129.3 (C2' and C6'), 129.4 (C3' and C5'), 129.6 (C7), 133.7 (C4), 138.1 (C3), 139.1 (C4'), 143.6 (C1'), 167.6 (C=O); HRMS (ESI) *m/z*, calcd. for $C_{17}H_{15}O_4NSCl^-$: 366.0381 and 364.0410, found: 366.0361 and 364.0381.

Methyl (*E*)-2-{[(4-fluorophenyl)sulfonamido]methyl}-3-phenylacrylate (**2d**)

Yield 89%; white solid; mp 70.8-71.5 °C; IR (ATR) ν_{max} / cm^{-1} 3257, 3066, 3030, 3005, 2950, 2842, 1700, 1440, 1338, 1155, 842, 774; ^{1}H NMR (300 MHz, $CDCl_3$) δ 3.77 (s, 3H, OCH$_3$), 3.99 (d, *J* 6.6 Hz, 2H, H1), 5.31 (t, *J* 6.3 Hz, 1H, NH), 7.10-7.16 (m, 2H, H3' and H5'), 7.35-7.43 (m, 5H, H5, H6, H7, H8 and H9), 7.74 (s, 1H, H3), 7.75-7.81 (m, 2H, H2' and H6'); ^{13}C NMR (75 MHz, $CDCl_3$) δ 40.5 (C1), 52.3 (OCH$_3$), 116.2 (d, *J* 22.4 Hz, C3' and C5'), 126.3 (C2), 128.8 (C5 and C9), 129.4 (C6 and C8), 129.6 (C4), 129.9 (d, *J* 9.2 Hz, C2' and C6'), 133.8 (C7), 135.6 (d, *J* 3.2 Hz, C1'), 143.5 (C3), 165.0 (d, *J* 253.4 Hz, C4'), 167.6 (C=O); HRMS (ESI) *m/z*, calcd. for $C_{17}H_{15}O_4NSF^-$: 348.0771, found: 348.0700.

Methyl (*E*)-3-phenyl-2-(phenylsulfonamidomethyl)acrylate (**2f**)

Yield 56%; white crystals; mp 102.2-102.5 °C; IR (ATR) ν_{max} / cm^{-1} 3442, 3273, 3058, 2944, 2880, 1706, 1325, 1166, 702, 691, 587, 572; ^{1}H NMR (300 MHz, $CDCl_3$) δ 3.75 (s, 3H, OCH$_3$), 3.99 (d, *J* 6.6 Hz, 2H, H1), 5.30 (t, *J* 6.3 Hz, 1H, NH), 7.35-7.41 (m, 5H, H5, H6, H7, H8 and H9), 7.45-7.50 (m, 2H, H3' and H5'), 7.55-7.59 (m, 1H, H4'), 7.73 (s, 1H, H3), 7.77-7.80 (m, 2H, H2' and H6'); ^{13}C NMR (75 MHz, $CDCl_3$) δ 40.5 (C1), 52.3 (OCH$_3$), 126.4 (C2), 127.2 (C6 and C8), 128.8 (C5 and C9), 129.0 (C3' and C5'), 129.5 (C2' and C6'), 129.54 (C7), 132.7 (C4), 133.8 (C4'), 139.5 (C1'), 143.5 (C3), 167.6 (C=O); HRMS (ESI) *m/z*, calcd. for $C_{17}H_{16}NO_4S^-$: 330.0801, found: 330.0750.

X-ray crystallography

X-ray diffraction measurement of the compound **1e** was performed on an Enraf-Nonius Kappa-CCD diffractometer (Delft, Holland) using graphite monochromated Mo Kα radiation (λ = 0.71073 Å) at room temperature (293 K). The collection software used was Bruker AXS Collect and the data processing was made with HKL Denzo-Scalepack program.[15] The structure was solved by direct methods

using SIR-92 program and the model was refined by full-matrix least-squares on F^2 with SHELXL-2018.[16,17] Absorption correction (multi-scan) was applied for the compound using the program SORTAV.[18]

The diffraction pattern of **2f** was collected at room temperature (293 K) on an XtaLAB Mini diffractometer (Houston, USA) using Mo Kα radiation monochromated by graphite. Using Olex2,[19] the structure was solved with the SHELXT structure solution program using Intrinsic Phasing and refined with the SHELXL-2018 refinement package using least squares minimization.[17]

For both compounds, all non-hydrogen atoms were refined using anisotropic displacement parameters. The hydrogen atoms in their calculated positions were refined using a riding model. Structural representations were drawn using ORTEP-3 and MERCURY.[20,21] Details of the unit cell, data collection and refinement are summarized in Table 1.

The complete data on the X-ray crystallographic analysis containing the atomic coordinates, bond lengths and bond angles have been deposited with the Cambridge Crystallographic Data Centre (CCDC No. 1936711 and 1997666, compounds **1e** and **2f**, respectively).

Hirshfeld surface

The Hirshfeld 3D surface was generated using a high (standard) surface resolution with the program Crystal Explorer 17.5.[22] The strength of the interactions was calculated by Hirshfeld d_{norm} surface (normalized contact distance). The 2D fingerprint plots were prepared for the analysis of the relative contribution of different intermolecular interactions of compounds **1e** and **2f**. The 3D d_{norm} surface was mapped using a color scale of −0.1000 to 1.0000. The shape index was mapped in the color range of −1.000 to 1.000 a.u. The 2D fingerprint plots were displayed using with the d_e and d_i distance scales displayed on the graph axes (0.6-2.8 Å). All hydrogen bond lengths were automatically modified to typical standard neutron values (C–H of 1.083 Å).

Energy frameworks and lattice energy calculations

Energy framework analysis was used to explore the intermolecular interaction energies between the molecules of the cluster within 3.8 Å. These calculations were

Table 1. Crystal data and the details of diffraction experiments for compounds **1e** and **2f**

Compound	**1e**	**2f**
Empirical formula	$C_{17}H_{16}N_2O_2S$	$C_{17}H_{17}NO_4S$
Formula weight / (g mol^{-1})	312.38	331.37
Temperature / K	293(2)	293(2)
Crystal system/space group	orthorhombic/Pcab	monoclinic/$P2_1/c$
a / Å	9.0612(4)	10.832(2)
b / Å	18.2037(5)	18.322(2)
c / Å	19.0473(7)	8.301(1)
β / degree	–	103.53(1)
Volume / Å^3	3141.8(2)	1601.8(4)
Z	8	4
Calculated density / (mg m^{-3})	1.332	1.374
Absorption coefficient / mm^{-1}	0.214	0.222
T_{min}/T_{max}	0.954/0.981	–
F(000)	1312	696
Crystal size / mm	0.225 × 0.201 × 0.088	0.254 × 0.223 × 0.095
θ range for data collection / degree	3.096-26.359	2.758-25.999
Limiting indices	0, 11; 0, 22; 0, 23	−13, 4; −22, 19; −10, 10
Reflections collected / unique	11404 / 3198 [*R*(int) = 0.062]	6049 / 3133 [*R*(int) = 0.059]
Observed reflections [I > 2σ(I)]	2408	1844
Parameters refined	199	208
Goodness-of-fit on F^2	1.072	1.117
Final *R* indices [I > 2σ(I)]	R = 0.0521, *wR* = 0.1519	R = 0.0818, *wR* = 0.2012
R indices (all data)	R = 0.0692, *wR* = 0.1613	R = 0.1392, *wR* = 0.2462
Max.; min. in Δρ map / (e Å^{-3})	0.531; –0.589	0.421; –0.562

$R_1 = \Sigma\,(||F_o| - |F_c||)/\Sigma|F_o|$; $wR_2 = [\Sigma w(|F_o^2| - |F_c^2|)^2/\Sigma w|F_o^2|^2]^{1/2}$; *a*-*c* and β: unit cell parameters; Z: number of molecules in the asymmetric unit; T: transmission factors; F(000): structure factor evaluated in the zeroth-order; θ: angle; *R*(int): internal error; I: intensity; σ: average of I; R: error; *wR*: overall weighted R factor; Δρ: residual electron density; F_o: observed structural factors; F_c: calculated structure factors.

performed using the Crystal Explorer 17.5 at Accurate mode (B3LYP (Becke, 3-parameter, Lee-Yang-Parr) using 6-31G(d,p) basis) (high performance),[22] with total interaction energy between any nearest neighbor molecular pairs given in terms of four components: electrostatic, polarization, dispersion, and repulsion, with scale factors of 1.057, 0.74, 0.871 and 0.618, respectively. The lattice energy calculation was done with cluster within 20 Å, using the same scale factors.

Computational calculations

DFT calculations were carried out using the B3LYP functional,[23,24] valence triple-zeta polarization (Def2-TZVP) basis set,[25] and Grimme's dispersion correction in Orca 4.0.[26,27] Structures were optimized using a 10^{-6} a.u. optimization criteria in forces and 10^{-8} a.u. in energy. Harmonic frequency analyses were carried out in the optimized structures to confirm that they are local minima in the potential energy surface. All calculations considered the solvent effect included through conductor-like polarizable continuum model (CPCM),[28] using a dielectric constant (ε) of 10.36, which corresponds to 1,2-dichloroethane, the solvent used in the syntheses. The molecular orbitals were plotted using an isovalue of 0.03 e^{-} au^{-3}.

Biological assay

The antifungal activity of the allyl sulfonamides was evaluated against *B. cinerea* by the poisoned food technique.[3] The potato dextrose agar (PDA) culture medium (Kasvi, São José dos Pinhais, Brazil) was previously sterilized in autoclave (Stermax, Pinhais, Brazil) for 20 min at 121 ºC. Glassware and spatulas were sterilized at 140 ºC for 3.5 h. The fungus was isolated from infected strawberry tissues with gray mold symptoms. Discs of *B. cinerea* mycelia (diameter of 7.4 mm) were placed on the center of Petri dishes containing 15 mL of PDA homogeneously mixed with the allyl sulfonamides **1a**-**1f** or **2a**-**2f** at three different concentrations (0.5, 1.5 and 3.0 mmol L^{-1}), and dimethyl sulfoxide (DMSO) and Tween 80 (LabSynth, Diadema, Brazil), 1% v/v each. Each sample was prepared in four repetitions and the dishes were kept in the incubator chamber (EthickTechnology, Vargem Grande Paulista, Brazil) at 22 ºC for three days. The control (negative check treatment) was prepared with PDA, DMSO and Tween 80 only. The diameter of the colony was measured with the aid of a digital caliper (Lee tools, Santo André, Brazil) on the third day of incubation. The percentages of inhibition were calculated in comparison with the control.

Results and Discussion

Synthesis and characterization

The twelve allyl sulfonamides **1a**-**1f** and **2a**-**2f** were prepared using the methodology shown in Scheme 1. The molecular formulae of the six unpublished allyl sulfonamides (**1a**, **2a-2d** and **2f**) were confirmed by HRMS-ESI, which presented the expected molecular ion peaks in the negative mode. The spectroscopic data obtained for **1b**-**1f** and **2e** are in accordance with the literature.[3,29,30]

Characteristic bands in the IR spectra of the allyl sulfonamides **1a**-**1f** and **2a**-**2f** indicated the presence of the most relevant groups within each structure. All spectra showed bands at 3301-3234, 1338-1307 and 1172-1139 cm^{-1} due to the N–H and the SO_2 groups (νNH, νSO_{2as} and νSO_{2sym}, respectively). The νC≡N band (2222-2207 cm^{-1}), observed in the spectra of **1a**-**1f**, and the νC=O band (1728-1700 cm^{-1}), present in the spectra of **2a**-**2f**, were the most important bands for the differentiation of the allyl sulfonamides series **1** and **2**.

In the ^{1}H NMR spectra of the MBH adducts (**1** and **2**, Scheme 1), two signals due to the sp^2-CH_2 methylenic hydrogens (H1) are observed at δ 6.02 and 6.10 when Y = CN, and at δ 5.81 and 6.32 when Y = CO_2Me.[14] In the spectra of **1a**-**1f** and **2a**-**2f**, these signals are substituted by one doublet at ca. δ 4 (H1) confirming the sp^3–CH_2–N bond formed upon the substitution reaction. Also, the signal for H3 at δ 5.28 or 5.54 in the spectra of **1** and **2** (Y = CN or CO_2Me, respectively) is shifted to δ 7.3-7.7 in the spectra of the allyl sulfonamides, showing that the double bond moved to C2=C3, with the elimination of the water molecule. Thus, the signals for C3 and C1 are observed at δ 138-146 and δ 40-47, respectively, in the ^{13}C NMR spectra of the allyl sulfonamides.

The C=O signal is observed at ca. δ 168 in the spectra of the compounds **2a**-**2f** and the CN signal appears at ca. δ 118 in the spectra of **1a**-**1f**. The signals of the aromatic carbons are duplicated in the spectrum of **2d**, with the expected C–F coupling constants of 253.4 Hz ($^1J_{C4'\text{-}F}$), 22.4 Hz ($^2J_{C3',C5'\text{-}F}$), 9.2 Hz ($^3J_{C2',C6'\text{-}F}$) and 3.2 Hz ($^4J_{C1'\text{-}F}$). Similar J values are observed for compound **1d**.[3]

X-ray crystallography

To gain a deeper insight into the structures of the allyl sulfonamides one compound of each series was investigated by single crystal X-ray diffraction. Thus, prism shaped white crystals of **1e** and **2f** were grown in chloroform/petroleum ether and acetone/water, respectively. The compound **1e**

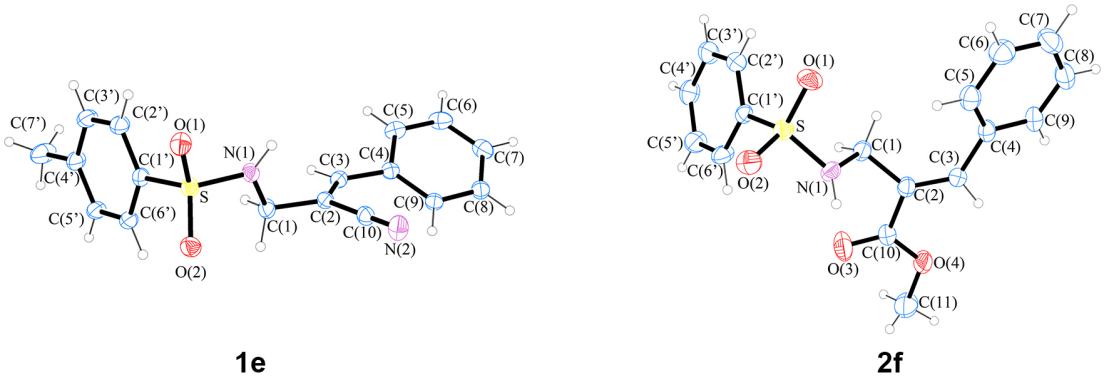

Figure 1. ORTEP view of compounds **1e** and **2f** with atom-numbering scheme and displacement ellipsoids drawn with 30% probability level.

crystallizes in the centrosymmetric space group Pcab of the orthorhombic system with eight molecules in the unit cell, while **2f** crystallizes in the centrosymmetric space group $P2_1/c$ of the monoclinic system with four molecules in the unit cell. The crystallographic asymmetric units of the compounds **1e** and **2f** are shown in Figure 1.

The X-ray data confirmed the proposed *Z*-configuration for compound **1e**, and the *E*-configuration for **2f** (Figure 1). The structural conformation of **1e** shows that the C2–C10≡N2 group is in the same direction of the SO_2 group, with a dihedral angle of just 5.90(1)° between the least-square plane through C1'SN1 groups and the line through C2C10. On the other hand, the ester group in **2f** is in the opposite direction with respect to the SO_2 group, the same dihedral angle being 139.68(1)°.

Table 2 shows selected bond lengths and angles for **1e** and **2f**. In order to check the molecular conformation parameters, both crystal structures were analyzed by Mogul software,[31] within The Cambridge Structural Database (CSD),[32] which allows us to compare all the bond lengths and angles of both structures with similar parameters found in the CSD for chemically equivalent compounds (Figures S1-S7, in the Supplementary Information (SI) section). This study shows that in both compounds the sulfur present a distorted tetrahedral geometry with S–C bond length very close to the expected mean value, 1.760 Å (Figure S1). The same does not occur with the other values. In this way, even when the S=O bond lengths in **1e** are close to the mean value (1.431 Å), the distance S–O1 in **2f** is considerable smaller (1.417(4) Å) showing the influences of the intermolecular interaction (Figure S2). The opposite behavior is observed in the case of the S–N bond. Both compounds present S–N values larger the mean value, 1.611 Å. However, the difference is higher for **1e**. This compound also presents a N1–C1 bond length significantly larger than the mean value (1.460 Å) in agreement with a clear intramolecular charge transfer to the SO_2 group induced by the intermolecular interaction (Figure S5).

The C1–C2 distance of ca. 1.505 Å is typical of a single bond, and the values observed for C2=C3 (ca. 1.310(3) Å) and C3–C4 (ca. 1.470 Å) are consistent with the conjugated π system.[33] The C–C bond lengths in the phenyl ring 1 (C1' to C6') and the phenyl ring 2 (C4 to C9) ranging from 1.366(9) to 1.402(3) Å are in the range of related aromatic compounds.[3]

In the compound **1e** (Table 2), the C10≡N2 bond length of 1.147(3) Å confirms the value for a triple bond, while the C1–N1 bond distance of 1.481(3) Å is in the range of a single bond.[34] The C2–C10 distance (1.439(3) Å) is consistent with reported values for analogous cyano allyl sulfonamides.[3,34] The C4'–C7' distance is close to values observed in similar compounds.[34,35]

In the compound **2f** (Table 2), the C10–O3 is a formal double bond, the C10–O4 bond presents intermediate character, while the C11–O4 bond length is in the normal range for a C–O single bond, as observed in related compounds.[9,36] The C2–C10 bond in **2f** (1.483(8) Å) is longer than in the compound **1e** due to the stronger electron-withdrawing effect of the nitrile compared to the carboxyl group.

In both compounds, the phenyl rings are essentially planar with root-mean-square deviations (r.m.s.d.) of 0.0077 Å for **1e** and 0.0055 Å for **2f** (ring 1), and of 0.0014 Å for **1e** and 0.0055 Å for **2f** (ring 2) from the least-squares plane defined by the atoms. The dihedral angle between these planes are 77.0(1)° for **1e** and 86.7(1)° for **2f**. In the compound **1e**, the deviation of the C7' atom to the ring 2 is of 0.015(4) Å. The C1–N1–S angle is greater than the value expected for the sp^3 N atom. In both compounds, the torsion angles C1'–S–N1–C1 and N1–C1–C2–C10 are significantly different (Table 2). These angles around the S–N1 and C1–C2 bonds describe the conformation of fragments in relation to phenyl rings.

The crystal packings of both compounds are stabilized by C–H···O intramolecular interactions as well as C–H···O and C–H···π intermolecular interactions. The crystal packing of **1e** also presents C–H···N hydrogen bonds (Table 3).

Table 2. Geometric parameters for **1e** and **2f**: selected bond lengths, angles and torsion angles

Compound	**1e**	**2f**
Bond length / Å		
S–O1	1.434(1)	1.416(4)
S–O2	1.430(2)	1.434(4)
S–N1	1.638(2)	1.620(4)
S–C1'	1.760(2)	1.758(5)
N1–C1	1.481(3)	1.470(6)
C1–C2	1.505(3)	1.505(7)
C2–C3	1.335(3)	1.327(7)
C3–C4	1.463(3)	1.476(8)
C2–C10	1.439(3)	1.483(8)
C4'–C7'	1.509(3)	–
N2–C10	1.147(3)	–
C10–O3	–	1.186(6)
C10–O4	–	1.317(6)
O4–C11	–	1.435(8)
Angle / degree		
N1–S–C1'	106.2(1)	106.1(2)
C1–N1–S	116.4(1)	116.4(3)
C1–C2–C3	122.0(2)	127.2(5)
N1–C1–C2	109.9(2)	111.9(4)
C2–C3–C4	129.0(2)	129.8(5)
Torsion angle / degree		
C1'–S–N1–C1	–63.2(2)	55.6(4)
N1–C1–C2–C10	63.7(2)	71.676)
S–N1–C1–C2	–165.6(2)	172.2(4)

Table 3. Hydrogen-bond geometry in the crystal structures of compounds **1e** and **2f**

D–H···A	d(D–H) / Å	d(H···A) / Å	d(D···A) / Å	< (D–H···A) / degree
Compound **1e**				
C1–H1B···O2	0.97	2.55	2.960(3)	103
C2'–H2'···O1	0.93	2.65	2.987(3)	102
C6'–H6'···O2	0.93	2.61	2.952(3)	103
C6–H6···N2^{i}	0.93	2.58	3.296(3)	133
C9–H9···O2^{ii}	0.93	2.68	3.466(3)	143
C3–H3···π1^{iii}	0.93	2.99	3.489(2)	115
C5'–H5'···π1^{iv}	0.93	2.73	3.541(2)	146
Compound **2f**				
C2'–H2'···O1	0.93	2.53	2.897(7)	104
C3–H3···O4	0.93	2.29	2.704(7)	106
C5'–H5'···O3^{v}	0.93	2.56	3.184(8)	125
C6'–H6'···O2^{vi}	0.93	2.51	3.413(8)	163
C11–H11A···π2^{vii}	0.96	2.75	3.511(8)	137

Symmetry codes: (i) –1 + x, y, z; (ii) 1 – x, –y, 2 – z; (iii) –x, –y, –z; (iv) ½ – x, y, ½ + z, (v) 1 – x, 1 – y, 2 – z, (vi) 1 – x, 1 – y, 1 – z, (vii) 1– x, ½ + y, ½ – z . π1 is the centroid of the C4 to C9 ring and π2 is the centroid of the C1' to C6' ring.

In the compound **1e**, the C6–H6···N2 and C9–H9···O2 intermolecular interactions form dimmers connected by translation in the *a* axis direction, generating $R_2^2(11)$ ring motifs.[37] These dimmers form chains in the *a* axis direction (Figure 2). Furthermore, two C–H···π interactions link these chains in the *c* axis direction into a three-dimensional supramolecular network. In the compound **2f**, the C5'–H5'···O3 intermolecular interactions form dimmers between molecules related by an inversion center, generating $R_2^2(20)$ ring motifs. These dimmers are interlinked by C6'–H6'···O2 interactions which also form dimmers between molecules related by an inversion center, generating $R_2^2(10)$ ring motifs, forming chains in the *c* axis direction (Figure 3). Furthermore, C–H···π interactions link these chains in the *a* axis direction into a bidimensional layers.

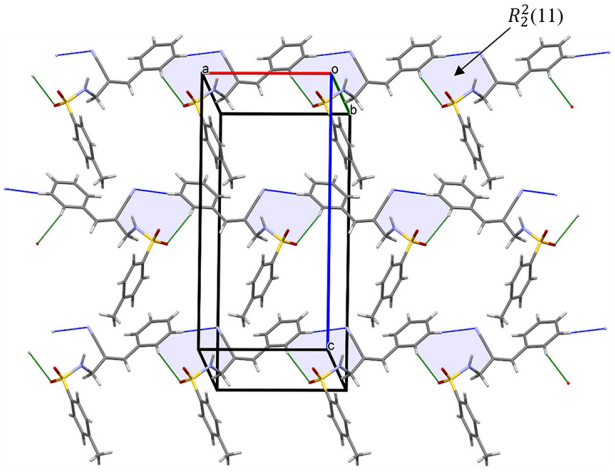

Figure 2. Structural packing of **1e** forming infinite chains along the *a* axis direction. Dashed blue lines indicate C–H···N and green lines indicate C–H···O intermolecular interactions.

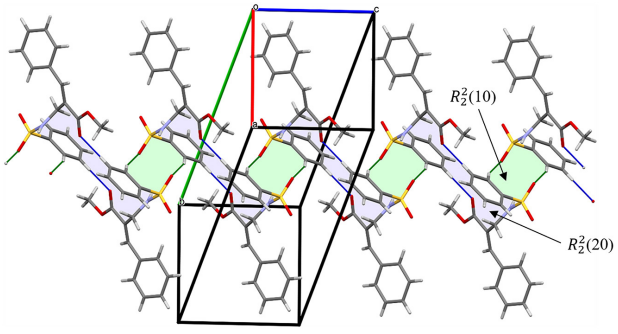

Figure 3. Structural packing of **2f** showing infinite chain along the *c* axis direction. Dashed blue lines indicate C5'–H5'···O3 and green lines indicate C6'–H6'···O2 intermolecular interactions.

Hirshfeld surface analysis

The Hirshfeld surface (HS) analysis provides an understanding of interactions in the formation of the supramolecular structure. The HS mapped with d_{norm}

for compounds **1e** and **2f**, shown in Figures 4 and 5, respectively, evidence dimers in the structural packing. The most intense red regions (stronger interactions) occur near to C–H···O and C–H···N interactions.

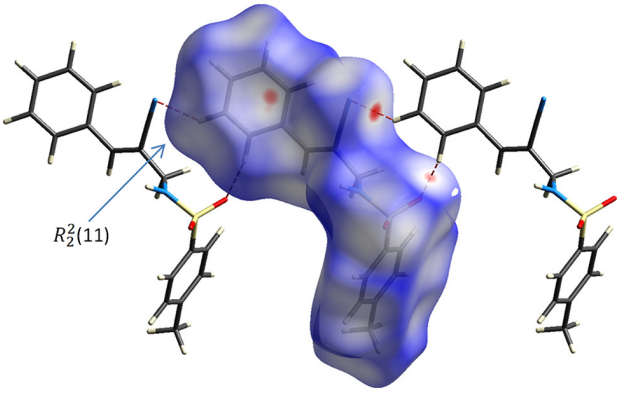

Figure 4. Hirshfeld surface mapped with d_{norm} for compound **1e**. The surface is partially transparent for clarity.

In order to visualize the participation of intermolecular interactions in the crystal structures of compounds **1e** and **2f**, the atom···atom interactions were further investigated by shape index and 2D fingerprint plots. The shape index depicted in Figure 6, allows to identify the complementarity between molecules in the crystal structure. Thus, the red dots indicate closer atoms, indicating interactions between neighboring molecules. These regions suggest significant C–H···π and C–H···O interactions, which are consistent with the X-ray analysis. The 2D fingerprint plots (Figure 7) are useful for analyzing the relative contribution of different intermolecular interactions in the crystal structures of **1e** and **2f**. These data show that

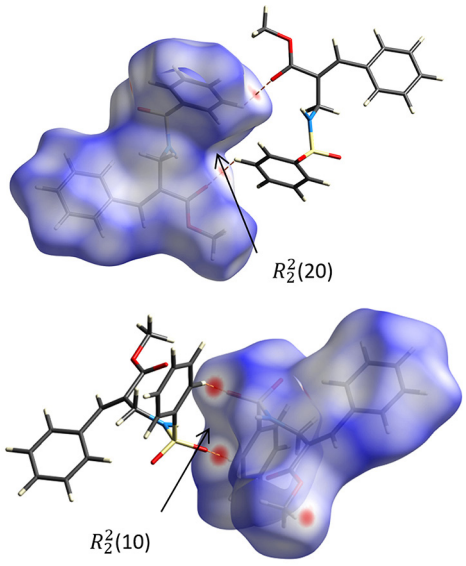

Figure 5. Hirshfeld surface mapped with d_{norm} for compound **2f**. The surface is partially transparent for clarity.

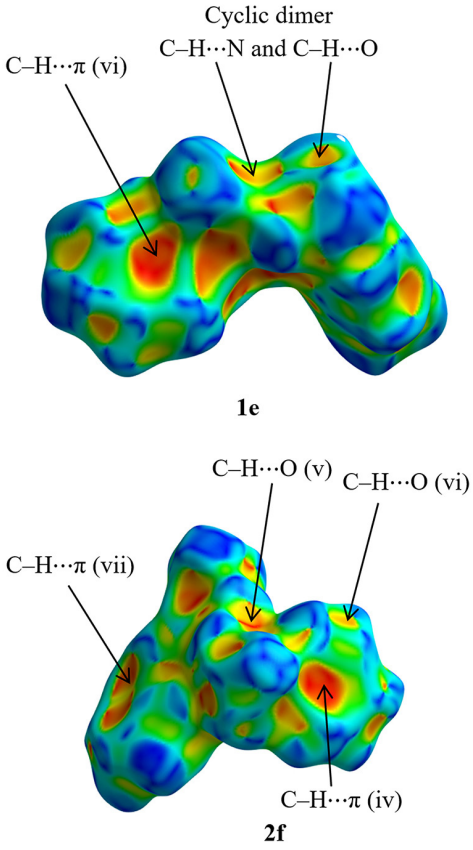

Figure 6. Hirshfeld surfaces mapped with shape index of compounds **1e** and **2f**.

the crystal structure of **1e** is determined by H···H, C···H, H···C, O···H, H···O, N···H and H···N contacts, whereas the structure of **2f** is determined by H···H, C···H, H···C, O···H and H···O contacts. The Figure 8 summarizes the selected percentages of contacts in the crystal structures of **1e** and **2f**. The non-classical H–H interactions constitute the most significant contribution to the total HS (39.1 and 46.6%, respectively for **1e** and **2f**). It is also important to highlight the N···H/H···N (13.0% in **1e** and ca. 0% in **2f**) and O···H/H···O (17.5% in **1e** and 24.8% in **2f**) contributions to the crystal packaging. The inspection of contacts between the other types of atoms pointed out that there are no significant π···π interactions within the crystals (C···C contacts make 3.1 and 1.7% of the surface area, respectively for **1e** and **2f**).

Energy framework calculation

The energy partitioning showed that the maximum contribution to the lattice stabilization is coming from the dispersion component, with contributions around 55% for **1e** and 53% for **2f**. The coulomb component contributes with ca. 34% in both compounds, the remaining contribution coming from the polarization energy. The

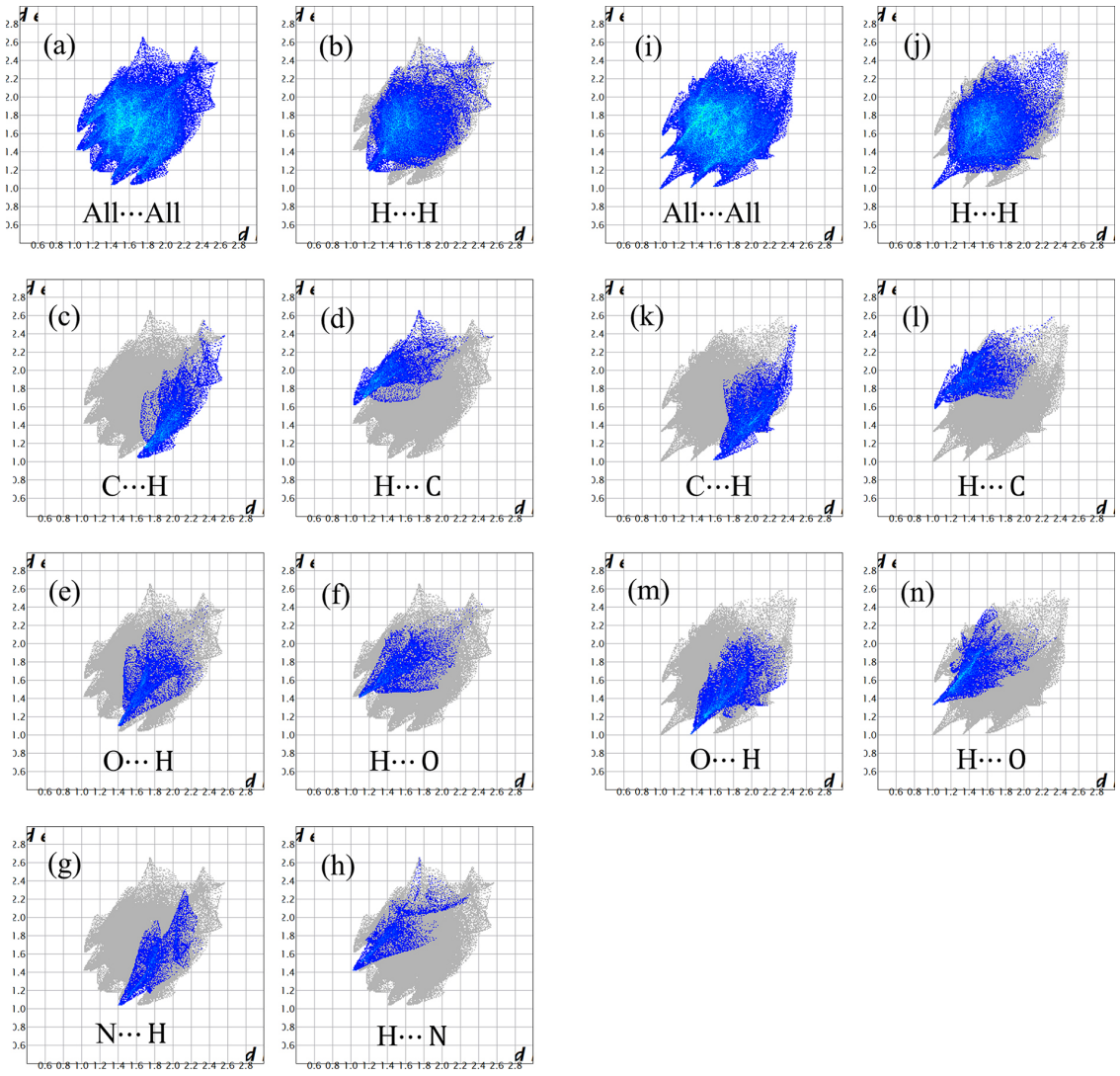

Figure 7. Two-dimensional fingerprint plots of compounds **1e** (a-h) and **2f** (i-n). The d_i and d_e distances values are shown in Å.

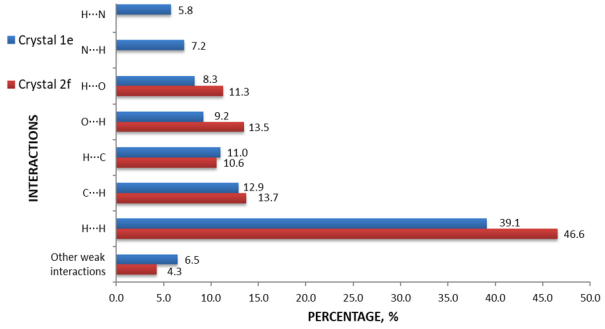

Figure 8. Percentages of contact interactions contributions to the Hirshfeld surface areas in compounds **1e** and **2f**.

electrostatic, polarization, dispersion, repulsion and total energy of interaction of these compounds are listed in Table 4. The Figures S8 and S9 in the SI section show these different intermolecular interactions, with the geometrical parameters and interaction energies partitioned into the energy components.

Through the analysis of the energy structure diagrams (Figures 9 and 10), it is possible to observe that the coulomb and dispersion terms of energy frameworks for both compounds indicate that they are similar. However, the dispersion term is more dominant when compared to the coulomb term.

The lattice energy (–336.5 and –333.6 kJ mol^{-1}, for **1e** and **2f**, respectively) showed that the expected relationship between the calculated lattice energy and the melting points are practically preserved. Thus, the highest energy in the network corresponds to the highest melting point, in this case, of the compound **1e**.

Molecular modeling

DFT calculations were carried out in the presence of a reaction field to simulate the solvent effect and provide an understanding about the geometrical structures in

Table 4. Total interaction energies of **1e** and **2f** partitioned into the energy components

Compound	E_{ele} / (kJ mol^{-1})	E_{pol} / (kJ mol^{-1})	E_{disp} / (kJ mol^{-1})	E_{rep} / (kJ mol^{-1})	E_{tot} / (kJ mol^{-1})
1e	–81.7	–7.1	–212.3	142.2	–188.6
2f	–66.4	–4.2	–218.8	14.1	–174.8

$E_{tot} = k_{ele}E_{ele} + k_{pol}E_{pol} + k_{dis}E_{dis} + k_{rep}E_{rep}$, where E_{tot}: total energy, k_{ele}: electrostatic constant, E_{ele}: electrostatic energy, k_{pol}: polarization constant, E_{pol}: polarization energy, k_{dis}: dispersion constant, E_{dis}: dispersion correction, k_{rep}: repulsion constant, and E_{rep}: repulsion energy.

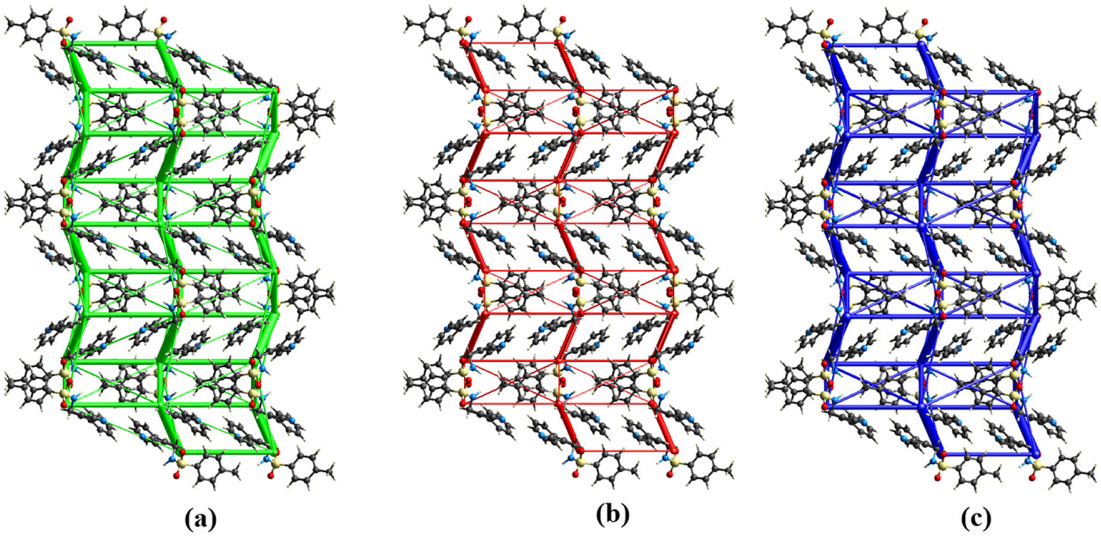

Figure 9. Energy frameworks corresponding to the different energy components (a) dispersion (green), (b) coulomb (red) and (c) total energy framework (blue) along *a* axis of compound **1e**. The tube size (scale factor) used in all the energy frameworks was 100 with 2 × 2 × 1 unit cells.

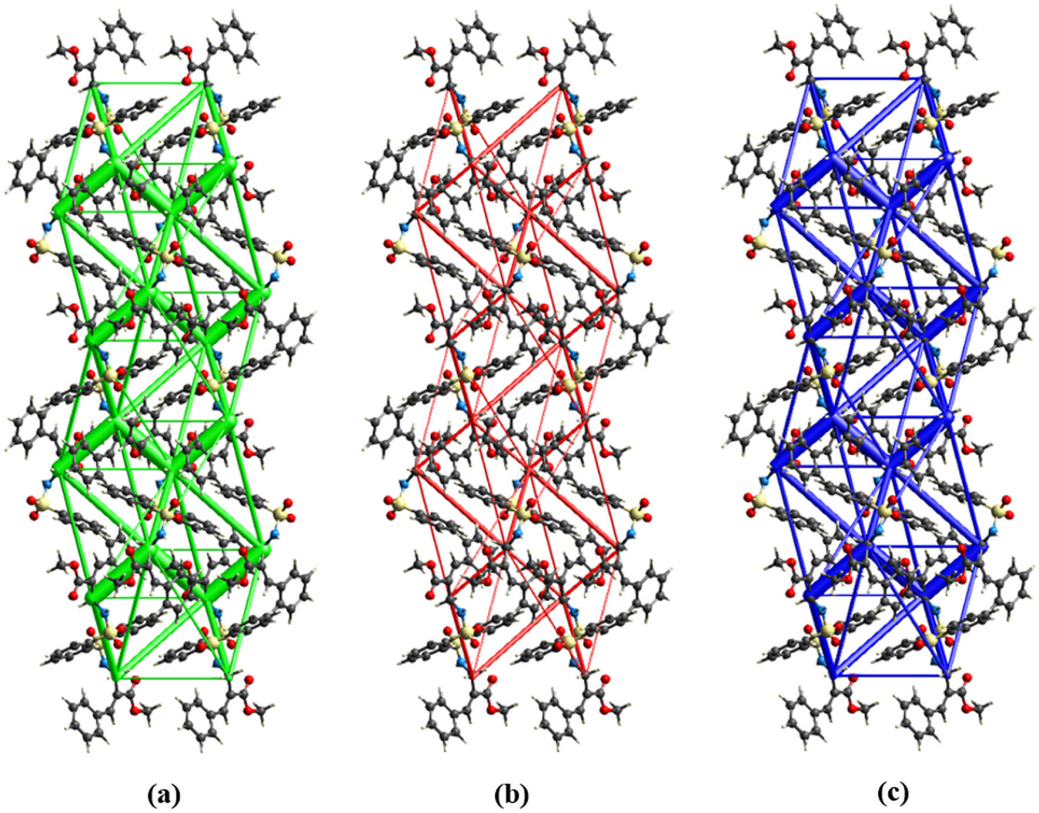

Figure 10. Energy frameworks corresponding to the different energy components (a) dispersion (green), (b) coulomb (red) and (c) total energy framework (blue) along *a* axis of compound **2f**. The tube size (scale factor) used in all the energy frameworks was 100 with 2 × 2 × 1 unit cells.

1,2-dichloroethane. The DFT calculations agree with the X-ray results. The main geometrical parameters for compounds **1a**-**1f** and **2a**-**2f** are highlighted in Table S1, in the SI section. The complete set of optimized structures for **1a**-**1f** and **2a**-**2f** are also provided (Figures S10 and S11) together with the optimized cartesian coordinates (Table S2). The atom numbering is the same used in the ORTEP diagram in Figure 1, for clarity.

The frontiers orbitals were also evaluated by the DFT calculations. For the compounds **1a**-**1f**, the gap between the highest occupied molecular orbital (HOMO) and lowest unoccupied molecular orbital (LUMO) is around 4.5-4.6 eV, with exception of **1a**, which gap is of 4.3 eV (Figure 11). The frontiers orbitals for the compound **1c** shown in Figure 12 are similar to those calculated for **1b**-**1f**. The results indicate that both HOMO and LUMO orbitals are typically antibonding orbitals, located in the aromatic ring and the nitrile. For compound **1a**, the HOMO orbital has some contribution from the p-orbital of iodine, as shown in Figure 12b, and there is a node plane between the iodine atom and the aromatic ring in this molecular orbital. This could be related to the different reactivity of this molecule towards the biological targets. It is also interesting to note the concentration of the LUMO orbital in the nitrile, indicating that this is the more susceptible site to a nucleophilic attack.

The calculated HOMO-LUMO gap for the esters **2a**-**2f** is in the range of 4.6-4.8 eV (Figure 11) and the frontier

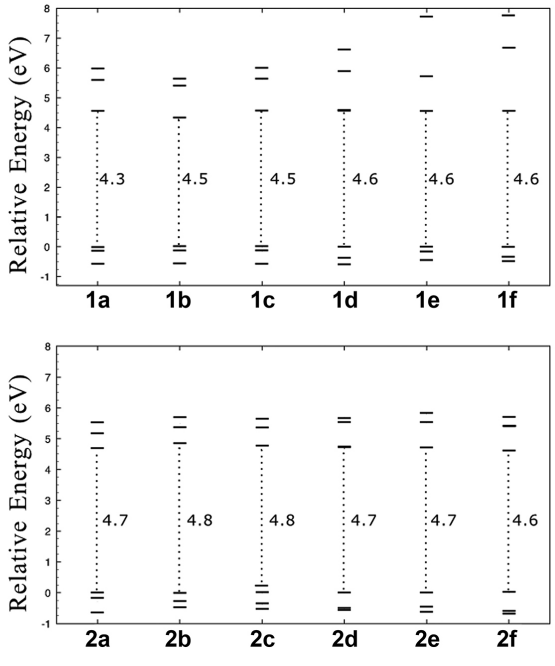

Figure 11. Diagram of frontiers molecular orbitals calculated at B3LYP/def2-TZVP level of theory with the HOMO-LUMO gap indicated in eV. The energy of each orbital is indicated in relation to HOMO, which was set to zero.

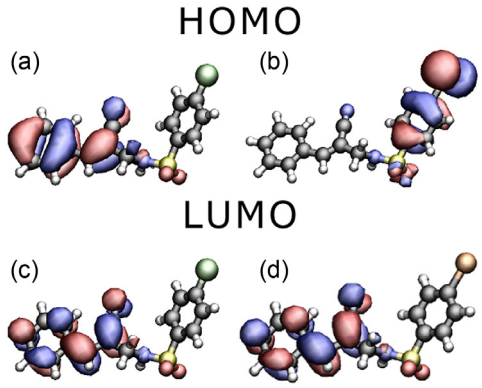

Figure 12. HOMO and LUMO orbitals calculated at B3LYP/Def2-TZVP level. (a) and (c) represent the orbitals of **1c**, which are similar to those calculated for **1b**-**1f**. (b) and (d) are the frontier orbitals of compound **1a**. The isosurface was set as 0.03 e^- $a.u^{-3}$. The atom color codes: C (black), H (white), N (blue), O (red), S (yellow), Cl (green), and I (orange).

orbitals are similar for all the components of the series, being antibonding orbitals located in the aromatic ring and the ester group, as exemplified in Figure 13 for the compound **2c**.

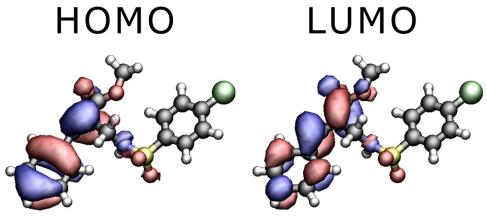

Figure 13. HOMO and LUMO orbitals calculated at B3LYP/Def2-TZVP level for the compound **2c**. The isosurface was set as 0.03 e^- $a.u^{-3}$. The atom color codes: C (black), H (white), N (blue), O (red), S (yellow), and Cl (green).

The synthetic route favors the formation of the diastereomers *Z* for the cyano compounds **1a**-**1f** and the *E* configuration for the ester compounds **2a**-**2f**. The DFT calculations confirm these isomers as the most stables in each series (Table 5).

It is important to highlight that the difference in energy between the *E* and *Z* forms for the series **2a**-**2f** is small, with the *E* isomer being, in most cases, less than 10 kJ mol^{-1} more stable than the *Z* isomer. In the series **1a**-**1f**, compounds **1b** and **1c** are remarkably more stable in the *Z* form (Table 5).

Antifungal assay

The cyano-sulfonamides **1b**, **1c**, **1d** and **1f** are active *in vitro* against *Colletotrichum gloeosporioides*, the causal agent of anthracnose in plants. They inhibit from 15% (**1b**) to 48% (**1f**) the mycelial growth of *C. gloeosporioides*, at the concentration of 1.5 mmol L^{-1}.[3] In this work, the influences of the twelve allyl sulfonamides in the mycelial

Table 5. Relative stability between the most stable diastereomer of each formula and the less stable isomer

	Relative stability / (kJ mol^{-1})					
	a	**b**	**c**	**d**	**e**	**f**
1	–6.0	–69.4	–35.6	–10.5	–6.7	–15.5
2	–4.6	–6.6	–4.0	–4.2	–15.6	–1.4

growth of *B. cinerea* were investigated through a similar methodology. Among the necrotrophic and polyphage fungi, *B. cinerea* is one of the most studied,[38] especially due to the occurrence of resistance to available fungicides.[10,39] The bioassay results are summarized in Table 6.

Table 6. Percentage inhibition of the mycelial growth of *B. cinerea* after three days of incubation at 22 °C in the presence of the allyl sulfonamides **1a-1f** and **2a-2f** in different concentrations with respect to the control

Treatment	Concentration / (mmol L^{-1})		
	0.5	1.5	3.0
	Inhibition ± SD / %		
1a	21.2 ± 0.6^{k}	36.9 ± 0.2^{g}	39.5 ± 2.4^{f}
1b	27.3 ± 1.3^{i}	36.8 ± 1.1^{g}	42.2 ± 0.7^{e}
1c	28.9 ± 0.3^{i}	38.8 ± 0.6^{f}	43.2 ± 0.2^{e}
1d	18.1 ± 0.4^{k}	35.2 ± 0.1^{g}	52.0 ± 0.7^{c}
1e	16.4 ± 2.9^{k}	39.0 ± 1.0^{f}	59.9 ± 0.5^{a}
1f	9.3 ± 3.7^{n}	16.3 ± 3.3^{k}	39.7 ± 4.0^{f}
2a	24.4 ± 5.7^{i}	44.4 ± 0.8^{e}	56.7 ± 0.7^{b}
2b	11.7 ± 1.0^{m}	32.0 ± 4.1^{h}	49.6 ± 2.2^{c}
2c	7.7 ± 0.4^{n}	35.9 ± 2.6^{g}	52.0 ± 3.0^{c}
2d	15.6 ± 0.2^{l}	22.0 ± 1.2^{j}	55.1 ± 0.2^{b}
2e	11.9 ± 0.9^{m}	32.0 ± 4.1^{h}	54.1 ± 0.2^{b}
2f	4.4 ± 0.4^{o}	47.7 ± 0.7^{d}	56.1 ± 1.3^{b}

Inhibition (%) = [(dc – 7.4) – (dt – 7.4)]/(dc – 7.4) × 100; where dc: average diameter (in mm) of the fungal colony in the control, dt: average diameter (in mm) of the fungal colony in the treatment, and 7.4 mm = diameter of the discs of mycelia. SD: standard deviation. Values followed by different letters are significantly different by the Scott-Knott test at 5% probability.

It is clear that the inhibition was dose dependent for all compounds. The activity becomes prominent at 3 mmol L^{-1}, where the inhibition percentages are close or superior to 50%. The results for each concentration are similar, showing that the variation of the groups X (I, Br, Cl, F, CH_3 or H) is of minor importance for the observed activity. Nevertheless, at 3 mmol L^{-1}, it was possible to differentiate the behavior of **1d** and **1e**, which presented the best results within the series **1a**-**1f**. The compounds **2d** and **2e**, are also among the most actives (**2a**, **2d-2f**) in this series, although the results were more homogeneous within the **2a**-**2f** series.

It seems that the ester group has a greater impact on the antifungal activity towards *B. cinerea* than the nitrile, as the results of the series **2a**-**2f** were, in general, superior to those of the series **1a**-**1f**, at 3 mmol L^{-1}. This behavior could be related to the differences in conformation of those groups (*trans* to the SO_2 group in **2f** and *cis* in **1e** in relation to the ester and cyano groups, respectively) as discussed in the X-ray crystallography sessions. In lower concentrations, the differentiation of the various compounds was less evident.

Conclusions

The reactions between MBH adducts and primary sulfonamides in the presence of sulfuric acid furnish allyl sulfonamides in good yields. The compounds **1a-1f** and **2a-2f** were synthesized and characterized by spectroscopy techniques and investigated by molecular modeling, and compounds **1e** and **2f** were also analyzed by single crystal X-ray. The DFT and X-ray diffraction studies confirmed that the reactions are stereospecific, providing the *Z*-configuration for the series of the cyano-sulfonamides **1a-1f** and *E*-configuration for the series of the carbomethoxy-sulfonamides **2a-2f**. Moreover, theoretical calculations confirmed that both HOMO and LUMO orbitals of these allyl sulfonamides are typically antibonding orbitals, located in the aromatic ring and in the nitrile or the ester group, with a unique difference observed for **1a**, which has a larger contribution of the iodine p orbital in the HOMO. The energy framework studies showed greater significance of the dispersion term and the calculated lattice energy is in agreement with the melting points. The crystal packing of **1e** is stabilized by C–H···O and C–H···π interactions while **2f** is stabilized by C–H···O, C–H···N and C–H···π interactions. The 2D fingerprint plots showed that in **1e**, the N···H/H···N and O···H/H···O interactions are the most important contacts for the crystal lattice stability, with a contribution of 30.5% for the HS area while in **2f**, the H···O/O···H contacts are important for the crystal lattice, with a contribution of 24.8% for the HS area. The energy partitioning showed that the maximum contribution to the lattice stabilization is coming from the dispersion component with contribution greater than 50% while the coulomb component contributes around 34%. The calculated lattice energy is in agreement with the melting points. The compounds inhibited the mycelial growth of the pathogenic fungus *B. cinerea*, with emphasis on the series **2a-2f** (50-60% inhibition) and

the compounds **1d**-**1e** (52-60% inhibition) at 3 mmol L^{-1} *in vitro*. The differences in the molecular configuration in these groups (*E* for **2a**-**2f** and *Z* for **1a**-**1f**) led to different intermolecular interactions, which might be related to the differences observed in the biological activity evaluated. Thus, the class of allyl sulfonamides present a potential application for the control of fungal diseases and is worth of further investigation.

Supplementary Information

Crystallographic data (excluding structure factors) for the structures in this work were deposited in the Cambridge Crystallographic Data Centre as supplementary publication number CCDC 1936711 and CCDC 1997666, compounds **1e** and **2f**, respectively. Copies of the data can be obtained, free of charge, via https://www.ccdc.cam.ac.uk/structures/.

Supplementary information (Figures S1-S11, Tables S1 and S2, NMR and infrared spectra of the new allyl sulfonamides **1a**, **2a-2d** and **2f** in the Figures S12-S29) is available free of charge at http://jbcs.sbq.org.br as PDF file.

Acknowledgments

We are grateful to the Coordenação de Aperfeiçoamento de Pessoal de Nível Superior (CAPES, Brazil, grant 001), Fundação de Amparo à Pesquisa do Estado de Minas Gerais (FAPEMIG, Brazil, grant APQ-02382-17) and Conselho Nacional de Desenvolvimento Científico e Tecnológico (CNPq, Brazil, J. E. grant No. 305190/2017-2), for financial support and research fellowships. We thank the Núcleo de Análise de Biomoléculas of the Universidade Federal de Viçosa for providing the facilities for HRMS experiments.

Author Contributions

A. S. Rabello was responsible for experimental syntheses, characterization of substances, antifungal assay, data curation, writing original draft, review and editing; M. M. M. Rubinger for research conceptualization, funding acquisition, project administration, investigation, data curation, supervision, formal analysis, writing original draft, manuscript submission, review and editing; R. A. C. Souza for X-ray crystallography data treatment, Hirshfeld surface and energy framework calculation, writing original draft, review and editing; S. Guilardi for X-ray crystallography data treatment, Hirshfeld surface and energy framework calculation, data curation, supervision, formal analysis, writing original draft and review; G. F. de Lima for molecular modeling and DFT calculations, writing original draft, review and editing; E. C. Tavares for conceptualization, laboratory synthesis and characterization of part of the substances, writing original draft, review and editing; E. P. Zanon for laboratory synthesis and characterization of some substances; G. N. R. Silva for preparation and characterization of one allylsulfonamide; L. Zambolim for supervision of the antifungal assay, resources, writing-review; J. Ellena for collection of the X-ray data, resources, data curation, X-ray crystallography discussion, writing-review.

References

1. Foye, W. O.; Lemke, T. L.; Williams, D. A.; *Principles of Medicinal Chemistry*, 7th ed.; Lippincott Williams & Wilkins: Philadelphia, 2013.
2. Remko, M.; *J. Mol. Struct.: THEOCHEM* **2010**, *944*, 34.
3. Tavares, E. C.; Rubinger, M. M. M.; Zacchi, C. H. C.; Silva, S. A.; Oliveira, M. R. L.; Guilardi, S.; Alcântara, A. F. D. C.; Piló-Veloso, D.; Zambolim, L.; *J. Mol. Struct.* **2014**, *1067*, 43.
4. Demir, Y.; Köksal, Z.; *Arch. Physiol. Biochem.* **2020**, *126*, 1.
5. Basavaiah, D.; Rao, P. D.; Hyma, R. S.; *Tetrahedron* **1996**, *52*, 8001.
6. Basavaiah, D.; Veeraraghavaiah, G.; *Chem. Soc. Rev.* **2012**, *41*, 68.
7. Albuini-Oliveira, N. M.; Rubinger, M. M. M.; Guilardi, S.; Souza, R. A. C.; Ellena, J.; Alvarez, N.; Tavares, E. C.; Zacchi, C. H. C.; Vidigal, A. E. C.; Lima, M. S.; Zambolim, L.; *J. Mol. Struct.* **2020**, *1214*, 128.
8. Bugaenko, D. I.; Karchava, A. V.; Yurovskaya, M. A.; *Chem. Heterocycl. Compd.* **2020**, *56*, 128.
9. Vidigal, A. E. C.; Rubinger, M. M. M.; da Silva, L. F.; Zambolim, L.; Pereira, A. B. D.; Guilardi, S.; Souza, R. A. C.; Ellena, J.; *J. Braz. Chem. Soc.* **2020**, *31*, 703.
10. Saito, S.; Michailides, T. J.; Xiao, C. L.; *Eur. J. Plant Pathol.* **2019**, *154*, 203.
11. Elad, Y.; Perlot, I.; Prado, A. M. C.; Stewart, A. In *Botrytis - The Fungus, the Pathogen and Its Management in Agricultural Systems*; Elad, Y.; Fillinger, S., eds.; Springer: Dordrecht, 2016, ch. 20.
12. de Simone, N.; Pace, B.; Grieco, F.; Chimienti, M.; Tyibilika, V.; Santoro, V.; Capozzi, V.; Colelli, G.; Spano, G.; Russo, P.; *Foods* **2020**, *9*, 1138.
13. Quirce, S.; Vandenplas, O.; Campo, P.; Cruz, M. J.; de Blay, F.; Koschel, D.; Moscato, G.; Pala, G.; Raulf, M.; Sastre, J.; Siracusa, A.; Tarlo, S. M.; Walusiak-Skorupa, J.; Cormier, Y.; *J. Allergy Clin. Immunol.* **2016**, *71*, 765.
14. Cai, J.; Zhou, Z.; Zhao, G.; Tang, C.; *Org. Lett.* **2002**, *4*, 4723.
15. Otwinowski, Z.; Minor, W. In *Methods in Enzymology*, 276th ed.; Carter Jr., C. W.; Sweet, R. M., eds.; Academic Press: New York, 1997.

16. Spek, A. L.; *Acta Crystallogr., Sect. D: Biol. Crystallogr.* **2009**, *D65*, 148.
17. Sheldrick, G. M.; *Acta Crystallogr., Sect. C: Struct. Chem.* **2015**, *C71*, 3.
18. Altomare, A.; Cascarano, G.; Giacovazzo, C.; Guagliardi, A.; *J. Appl. Crystallogr.* **1994**, *27*, 435.
19. Dolomanov, O. V.; Bourhis, L. J.; Gildea, R. J.; Howard, J. A. K.; Puschmann, H.; *J. Appl. Crystallogr.* **2009**, *42*, 339.
20. Farrugia, L. J.; *J. Appl. Crystallogr.* **2012**, *45*, 849.
21. Macrae, C. F.; Edgington, P. R.; Mccabe, P.; Pidcock, E.; Shields, G. P.; Taylor, R.; Towler, M.; Streek, J. V. D.; *J. Appl. Crystallogr.* **2006**, *39*, 453.
22. Wolff, S. K.; Grimwood, D. J.; McKinnon, J. J.; Jayatilaka, D.; Spackman, M. A.; *Crystal Explorer* 2.1, *Program for Crystal Structure Refinement*; University of Western Australia, Australia, 2007.
23. Becke, A. D.; *Phys. Rev. A* **1988**, *38*, 3098.
24. Lee, C.; Yang, W.; Parr, R. G.; *Phys. Rev. B* **1988**, *37*, 785.
25. Weigend, F.; Ahlrichs, R.; *Phys. Chem. Chem. Phys.* **2005**, *7*, 3297.
26. Grimme, S.; Antony, J.; Ehrlich, S.; Krieg, H.; *J. Chem. Phys.* **2010**, *132*, 154104.
27. Neese, F.; *WIREs Comput. Mol. Sci.* **2018**, *8*, e1327.
28. Klamt, A.; Schuurmann, G.; *J. Chem. Soc., Perkin Trans. 2* **1993**, 799.
29. Kim, H. S.; Lee, H. S.; Kim, J. N.; *Bull. Korean Chem. Soc.* **2009**, *30*, 941.
30. Saikia, M.; Sarma, J. C.; *Can. J. Chem.* **2010**, *88*, 1271.
31. Bruno, I. J.; Cole, J. C.; Kessler, M.; Luo, J.; Momerwell, W. D. S.; Purkis, L. H.; Smith, B. R.; Taylor, R.; Cooper, R. I.; Harris, S. E.; Orpen, A. G.; *J. Chem. Inf. Comput. Sci.* **2004**, *44*, 2133.
32. Groom, C. R.; Bruno, I. J.; Lightfoot, M. P.; Ward, S. C.; *Acta Crystallogr., Sect. B: Struct. Sci., Cryst. Eng. Mater.* **2016**, *72*, 171.
33. Allen, F. H.; Kennard, O.; Watson, D. G.; Brammer, L.; Orpen, A. G.; *J. Chem. Soc., Perkin Trans. 2* **1987**, S1.
34. Souza, R. A. C.; Guilardi, S.; Rubinger, M. M. M.; Terra, L. R.; Tavares, E. C.; Ellena, J. A.; *J. Struct. Chem.* **2018**, *59*, 1192.
35. Vembu, N.; Garrison, J.; Youngs, W. J.; *Acta Crystallogr., Sect. E: Crystallogr. Commun.* **2003**, *E59*, o936.
36. Tavares, E. C.; Rubinger, M. M. M.; Filho, E. V.; Oliveira, M. R. L.; Ellena, J.; Guilardi, S.; Souza, R. A. C.; *J. Mol. Struct.* **2016**, *1106*, 130.
37. Etter, M. C.; *Acc. Chem. Res.* **1990**, *23*, 120.
38. Choquer, M.; Fournier, E.; Kunz, C.; Levis, C.; Pradier, J.; Simon, A.; Viaud, M.; *FEMS Microbiol. Lett.* **2007**, *277*, 1.
39. Yin, D.; Chen, X.; Hamada, M. S.; Yu, M.; Yin, Y.; Ma, Z.; *Eur. J. Plant Pathol.* **2015**, *141*, 169.

Submitted: April 12, 2021
Published online: June 30, 2021